bioRxiv preprint doi: https://doi.org/10.1101/620922; this version posted April 28, 2019. The copyright holder for this preprint (which was not certified by peer review) is the author/funder, who has granted bioRxiv a license to display the preprint in perpetuity. It is made available under aCC-BY-NC-ND 4.0 International license.

1 To mBio (Research article)

2 Behaviors and Energy Source of *Mycoplasma gallisepticum* Gliding

3

4 Masaki Mizutani,[a] Makoto Miyata[a,b]#

5

6 [a]Graduate School of Science, Osaka City University, Sumiyoshi-ku, Osaka, Japan

7 [b]The OCU Advanced Research Institute for Natural Science and Technology

8 (OCARINA), Osaka City University, Sumiyoshi-ku, Osaka, Japan

9

10 Running Title: *Mycoplasma* gliding behaviors

11

12

13 # Address correspondence to Makoto Miyata, miyata@sci.osaka-cu.ac.jp

14

15

16

bioRxiv preprint doi: https://doi.org/10.1101/620922; this version posted April 28, 2019. The copyright holder for this preprint (which was not certified by peer review) is the author/funder, who has granted bioRxiv a license to display the preprint in perpetuity. It is made available under aCC-BY-NC-ND 4.0 International license.

17 ABSTRACT

18 *Mycoplasma gallisepticum*, an avian-pathogenic bacterium, glides on host tissue
19 surfaces by using a common motility system with *Mycoplasma pneumoniae*. In the
20 present study, we observed and analyzed the gliding behaviors of *M. gallisepticum* in
21 detail by using optical microscopes. *M. gallisepticum* glided at a speed of 0.27 ± 0.09
22 μm/s with directional changes relative to the cell axis of 0.6 ± 44.6 degrees/5 s without
23 the rolling of the cell body. To examine the effects of viscosity on gliding, we analyzed
24 the gliding behaviors under viscous environments. The gliding speed was constant in
25 various concentrations of methylcellulose but was affected by Ficoll. To investigate the
26 relationship between binding and gliding, we analyzed the inhibitory effects of
27 sialyllactose on binding and gliding. The binding and gliding speed sigmoidally
28 decreased with sialyllactose concentration, indicating the cooperative binding of the cell.
29 To determine the direct energy source of gliding, we used a membrane-permeabilized
30 ghost model. We permeabilized *M. gallisepticum* cells with Triton X-100 or Triton
31 X-100 containing ATP and analyzed the gliding of permeabilized cells. The cells
32 permeabilized with Triton X-100 did not show gliding; in contrast, the cells
33 permeabilized with Triton X-100 containing ATP showed gliding at a speed of 0.014 ±
34 0.007 μm/s. These results indicate that the direct energy source for the gliding motility

bioRxiv preprint doi: https://doi.org/10.1101/620922; this version posted April 28, 2019. The copyright holder for this preprint (which was not certified by peer review) is the author/funder, who has granted bioRxiv a license to display the preprint in perpetuity. It is made available under aCC-BY-NC-ND 4.0 International license.

of *M. gallisepticum* is ATP.

IMPORTANCE

Mycoplasmas, the smallest bacteria, are parasitic and occasionally commensal. *Mycoplasma gallisepticum* is related to human pathogenic *Mycoplasmas*—*Mycoplasma pneumoniae* and *Mycoplasma genitalium*—which causes so-called 'walking pneumonia' and non-gonococcal urethritis, respectively. These *Mycoplasmas* trap sialylated oligosaccharides, which are common targets among influenza viruses, on host trachea or urinary tract surfaces and glide to enlarge the infected areas. Interestingly, this gliding motility is not related to other bacterial motilities or eukaryotic motilities. Here, we quantitatively analyze cell behaviors in gliding and clarify the direct energy source. The results provide clues for elucidating this unique motility mechanism.

INTRODUCTION

Members of the bacterial class Mollicutes, including the genus *Mycoplasma*, are parasitic, occasionally commensal, and characterized by small cells and genomes as well as the absence of a peptidoglycan layer (1, 2). More than ten *Mycoplasma* species, such as the fish pathogen *Mycoplasma mobile* (3-5) and the human pathogen

bioRxiv preprint doi: https://doi.org/10.1101/620922; this version posted April 28, 2019. The copyright holder for this preprint (which was not certified by peer review) is the author/funder, who has granted bioRxiv a license to display the preprint in perpetuity. It is made available under aCC-BY-NC-ND 4.0 International license.

Mycoplasma pneumoniae (6-8), have membrane protrusions and exhibit gliding motility in the direction of the membrane protrusion on solid surfaces, which enables *Mycoplasmas* to parasitize higher animals.

Interestingly, *Mycoplasma* gliding does not involve flagella or pili and is entirely unrelated to other bacterial motility systems and the conventional motor proteins that are common in eukaryotic motility systems (9, 10).

The gliding motilities of *Mycoplasmas* are classified into two systems; *M. mobile*-type and *M. pneumoniae*-type (5, 8). *M. pneumoniae*-type gliding has until now been studied mainly in *M. pneumoniae* and *Mycoplasma genitalium*. A structure outline of the gliding machinery has been suggested, including that for fifteen component proteins (6-8, 11). The gliding machinery, called the 'attachment organelle,' is composed of an internal core and adhesin complexes (12-14). The internal core is divided into three parts, the bowl complex, paired plates, and terminal button (3, 6, 13-15). It has been suggested that the bowl complex connects the internal core to the cell body and may be responsible for the generation or transmission of force (8, 16, 17). Furthermore, paired plates are the scaffold for formation and force transmission of the gliding machinery (8, 18-24). The terminal button is thought to tightly bind to the front side of the cell membrane (8, 23, 25-27). The adhesin complex is composed of P1 adhesin and P90 (28).

bioRxiv preprint doi: https://doi.org/10.1101/620922; this version posted April 28, 2019. The copyright holder for this preprint (which was not certified by peer review) is the author/funder, who has granted bioRxiv a license to display the preprint in perpetuity. It is made available under aCC-BY-NC-ND 4.0 International license.

71 P90 is encoded in tandem with P1 adhesin and is cleaved from another protein, P40, for
72 maturation (29, 30). A recent study shows that the homolog of P40/P90 in *M. genitalium*,
73 P110, has a binding pocket of sialylated oligosaccharides (SOs) (31), which are binding
74 targets for *Mycoplasma* infection and gliding. The mechanism of the gliding motility
75 has been proposed as an 'inchworm model,' in which a cell catches SOs on solid
76 surfaces through the adhesin complexes and is propelled by the repetitive extensions
77 and retractions of the internal core (3, 7, 8).
78 The gliding motility of *M. mobile* is driven by ATP using 'ghost' which has a
79 permeabilized membrane and can be reactivated by the addition of ATP (32-34). In
80 contrast, the direct energy source for *M. pneumoniae*-type gliding motility is still
81 unclear (8).
82 *Mycoplasma gallisepticum* is an avian pathogen that causes chronic respiratory disease
83 in chickens and infectious sinusitis in turkeys. The cells transmit from breeder birds to
84 their progeny *in ovo* (1, 35, 36). *M. gallisepticum* glides using the *M. pneumoniae*-type
85 motility system and has eight homologs of component proteins of gliding machinery in
86 *M. pneumoniae* whose identities for amino acids range from 20% to 45% (36-39). The
87 structure of the gliding machinery is similar to that in *M. pneumoniae* (37, 39). *M.*
88 *gallisepticum* has a faster growth rate and more stable cell shape than *M. pneumoniae*,

bioRxiv preprint doi: https://doi.org/10.1101/620922; this version posted April 28, 2019. The copyright holder for this preprint (which was not certified by peer review) is the author/funder, who has granted bioRxiv a license to display the preprint in perpetuity. It is made available under aCC-BY-NC-ND 4.0 International license.

which is beneficial for the motility study (37).

In this study, we observe and analyze the gliding behaviors of *M. gallisepticum* in detail, and clarify the direct energy source of the gliding motility by modified gliding ghost experiments.

RESULTS

Gliding behaviors

The gliding motility of *M. gallisepticum* has been reported previously (37, 40), but the details have not yet been examined. Therefore, these details were examined in this study. *M. gallisepticum* cells were collected, suspended in phosphate-buffered saline (PBS) containing 10% non-heat-inactivated horse serum, and inserted into a tunnel chamber constructed by taping coverslips and precoated with non-heat-inactivated horse serum and bovine serum albumin. Then, the tunnel chamber was washed with PBS containing 20 mM glucose (PBS/G) and was observed by phase-contrast microscopy. The cells showed a flask shape (Fig. 1A) and glided in the direction of the tapered end, as previously reported (Fig. 1B; see Movie S1 in the supplemental material) (37). The proportions of gliding cells to all cells and the gliding speeds averaged for 60 s at 1 s intervals were 62% ± 6% (n = 454) and 0.27 ± 0.09 μm/s (n = 231), respectively (Fig.

bioRxiv preprint doi: https://doi.org/10.1101/620922; this version posted April 28, 2019. The copyright holder for this preprint (which was not certified by peer review) is the author/funder, who has granted bioRxiv a license to display the preprint in perpetuity. It is made available under aCC-BY-NC-ND 4.0 International license.

1B and C), which is consistent with those reported in the previous study (37). To analyze the gliding direction, we traced the angles between the cell axis and the following gliding direction for 60 s at 5 s intervals, as previously described (41). The averaged gliding direction relative to the cell axis was 0.6 ± 44.6 degrees/5 s (n = 231) (Fig. 1D), indicating that *M. gallisepticum* has no significant directional bias.

Possibility of rolling around the cell axis

A previous study shows that the adhesin complexes of *M. pneumoniae* exist around the membrane protrusion (7). *M. gallisepticum* may have a similar distribution because it uses similar gliding machinery to *M. pneumoniae* (36-39). The distribution of adhesin complexes suggests that cells may roll around the cell axis during gliding. To examine this possibility, we traced the movement of 40 nm colloidal gold attached to a gliding cell. *M. gallisepticum* cells were biotinylated on the cell surface through amino groups, then mixed with 40 nm colloidal gold conjugated with streptavidin in the tunnel chamber and observed by dark-field microscopy. The cells attached with colloidal gold glided at a similar speed to cells without colloidal gold (see Fig. S1 and Movie S2 in the supplemental material). All pairs of mass centers of cells and colloidal gold moved while maintaining a constant distance (n = 20) (Fig. 1E; see Fig. S1 in the supplemental material), showing that the cells glide without rolling of the cell body.

bioRxiv preprint doi: https://doi.org/10.1101/620922; this version posted April 28, 2019. The copyright holder for this preprint (which was not certified by peer review) is the author/funder, who has granted bioRxiv a license to display the preprint in perpetuity. It is made available under aCC-BY-NC-ND 4.0 International license.

125 **Gliding in viscous environments**

126 A previous study shows that *M. mobile* gliding is drastically inhibited by viscous
127 environments created using methylcellulose (MC) or Ficoll (41). To examine the effects
128 of viscosity on *M. gallisepticum* gliding, we analyzed the gliding behaviors under
129 viscous buffers including MC or Ficoll. MC is a long, linear, and slightly branched
130 polymer, and forms a gel-like three-dimensional network. Ficoll is a highly branched
131 polymer which increases viscosity and does not form a network (42, 43). *M.*
132 *gallisepticum* cells were suspended in PBS/G containing various concentrations of MC
133 or Ficoll, inserted into the tunnel chamber, observed by phase-contrast microscopy, and
134 analyzed for gliding speed and direction (Fig. 2A). The gliding speed did not
135 significantly change with an increase in viscosity from 0.22 ± 0.06 μm/s (n = 50) at 0.66
136 mPa s to 0.19 ± 0.04 μm/s (n = 50) at 7.3 mPa s with 0% and 0.50% MC, respectively.
137 However, the gliding speed did significantly decrease to 0.11 ± 0.04 μm/s (n = 50) at 4.6
138 mPa s with 15% Ficoll ($P<0.001$ by Student's *t*-test) (Fig. 2B and C). The averaged
139 gliding direction relative to the cell axis did not change significantly with an increase in
140 viscosity for all examined conditions. However, the standard deviations of gliding
141 direction significantly decreased in Ficoll conditions ($P<0.001$ by F-test) from 27.4
142 degrees/5 s (n = 48) in 0% to 12.4 degrees/5 s (n = 50) in 15% Ficoll (Fig. 2B and C).

bioRxiv preprint doi: https://doi.org/10.1101/620922; this version posted April 28, 2019. The copyright holder for this preprint (which was not certified by peer review) is the author/funder, who has granted bioRxiv a license to display the preprint in perpetuity. It is made available under aCC-BY-NC-ND 4.0 International license.

These results indicate that the gliding motility of *M. gallisepticum* is affected by Ficoll but not MC.

Inhibition of binding and gliding by free sialyllactose

Previous studies show that *M. mobile* glides via dozens of working legs, the numbers of which can be reduced by the addition of free SOs (33, 44-46). To examine the relationship between binding and gliding, we added various concentrations of free 3′-*N*-acetylneuraminyllactose (3′-sialyllactose, SL), an SO, to gliding *M. gallisepticum* cells. The cell suspension was inserted into the tunnel chamber and observed by phase-contrast microscopy. After 60 s, the buffer was replaced by the buffers containing 0□0.5 mM SL. The gliding cells slowed down after the addition of free SL, and some of them detached from the glass surface (Fig. 3A and B). Most of the cells stopped for gliding kept binding to the end of the membrane protrusion (see Fig. S2 in the supplemental material). The inhibition ratio for binding was calculated from the number of gliding cells at 40 s after the addition of SL to the number before the SL treatments (45). The ratio decreased with SL concentration from 88% ± 11% (n = 14) in 0 mM to 13% ± 11% (n = 21) in 0.5 mM SL (Fig. 3C). The gliding speed at 40 s after the addition of SL also decreased with SL concentration, from 0.17 ± 0.06 μm/s (n = 58) in 0 mM to 0.06 ± 0.04 μm/s (n = 54) in 0.5 mM SL (Fig. 3D). The Hill constant of

bioRxiv preprint doi: https://doi.org/10.1101/620922; this version posted April 28, 2019. The copyright holder for this preprint (which was not certified by peer review) is the author/funder, who has granted bioRxiv a license to display the preprint in perpetuity. It is made available under aCC-BY-NC-ND 4.0 International license.

161 binding was calculated as previously described (45) to be about 1.55 (see Fig. S3 in the
162 supplemental material), indicating cooperativity in binding between cells and SL.

163 **Gliding ghost**

164 Previous studies show that the gliding motility of *M. mobile* is driven by ATP hydrolysis
165 based on gliding ghost experiments. In these experiments, *M. mobile* cells were
166 permeabilized with Triton X-100 and stopped for gliding. Gliding was then reactivated
167 by the addition of ATP (32-34). In contrast, the reactivation of permeabilized cells of *M.*
168 *pneumoniae*-type gliding *Mycoplasmas* has not been successful so far (8). At first, the
169 same method was tried for *M. gallisepticum*, but about half of the cells permeabilized
170 with Triton X-100 detached from the glass surfaces after the addition of ATP solution.
171 Cells were permeabilized with Triton X-100 and ATP to efficiently observe the
172 behaviors of permeabilized cells in the presence of ATP. This strategy was applied to *M.*
173 *mobile* to confirm whether it was efficient. Cultured *M. mobile* cells were suspended in
174 bufferA (10 mM HEPES pH 7.4, 100 mM NaCl, 2 mM $MgCl_2$, 1 mM EGTA, 1 mM
175 DTT, 0.1% MC) containing 20 mM glucose and inserted into the tunnel chamber. Then,
176 the cells were permeabilized with 0.013% Triton X-100 containing 1 mM ATP + 0.01
177 mM ADP or 1 mM ADP. The cells permeabilized with Triton X-100 containing 1 mM
178 ATP + 0.01 mM ADP glided at a similar speed to the intact cells. The cells

bioRxiv preprint doi: https://doi.org/10.1101/620922; this version posted April 28, 2019. The copyright holder for this preprint (which was not certified by peer review) is the author/funder, who has granted bioRxiv a license to display the preprint in perpetuity. It is made available under aCC-BY-NC-ND 4.0 International license.

179 permeabilized with Triton X-100 containing 1 mM ADP stopped gliding when they
180 were permeabilized (see Movie S3 and S4 in the supplemental material). These results
181 indicate that this method works efficiently. This method was then applied to *M.*
182 *gallisepticum*. Cultured *M. gallisepticum* cells were suspended in bufferA containing
183 10% non-heat-inactivated horse serum, inserted into the tunnel chamber, washed by
184 bufferA containing 20 mM glucose, and observed by phase-contrast microscopy. Under
185 these conditions, the proportion of gliding cells to all cells and the averaged gliding
186 speed were 74% ± 3% (n = 2011) and 0.36 ± 0.06 μm/s (n = 220), respectively (see Fig.
187 S4 in the supplemental material). The buffer was then replaced by 0.007% Triton X-100
188 containing no ATP, 1 mM ATP + 0.01 mM ADP, or 1 mM ADP in bufferA. The cells
189 became round at 10□30 s from the addition of Triton solutions (Fig. 4A and B) causing
190 the gliding speeds to decrease (Fig. 4C; see Fig. S5 in the supplemental material). The
191 round cells showed three levels of cell-image density shifts; (i) the image density did
192 not decrease, (ii) the image density decreased to be about 75% of the intact cell, (iii) the
193 image density decreased to half of the intact cell (Fig 4D and E; see Fig. S5 in the
194 supplemental material). The cells which decreased to be about 75% of the cell-image
195 density showed slow gliding when they were permeabilized with Triton X-100
196 containing 1 mM ATP + 0.01 mM ADP (Fig. 4A and C; see Fig. S5 and Movie S5 in the

bioRxiv preprint doi: https://doi.org/10.1101/620922; this version posted April 28, 2019. The copyright holder for this preprint (which was not certified by peer review) is the author/funder, who has granted bioRxiv a license to display the preprint in perpetuity. It is made available under aCC-BY-NC-ND 4.0 International license.

197 supplemental material). The cells permeabilized with Triton X-100 containing no ATP
198 or 1 mM ADP solution did not show gliding (n_{intact} = 3943 and 2604, respectively) (Fig.
199 4F). These results indicate that we succeeded in forming gliding ghosts of *M.*
200 *gallisepticum*. The occurrence ratio of gliding ghosts was calculated to be 0.41% from
201 the numbers of gliding ghosts and intact cells before Triton treatment (n_{intact} = 11528
202 and n_{ghost} = 47). The gliding speed of ghosts in 1 mM ATP + 0.01 mM ADP was
203 averaged for 150 s at 10 s intervals and found to be 0.014 ± 0.007 μm/s (Fig. 4G). The
204 62.9% of gliding ghosts continued to glide for 17 min of video recording. In the ATP
205 hydrolysis cycle, the ATP state becomes the ADP or P_i state through the ADP + P_i state.
206 Vanadate ion (V_i) with ADP can mimic the ADP + P_i state. V_i acts as a phosphate analog
207 to form an ADP-V_i complex which occupies the catalytic site of ATPase and blocks the
208 hydrolysis cycle (47, 48). The cells were permeabilized with Triton containing 1 mM
209 ATP + 0.5 mM V_i to examine whether V_i affects the gliding of ghosts, (Fig. 4F). The
210 gliding ghosts in ATP + V_i glided with 0.011 ± 0.010 μm/s (n = 9) at an occurrence ratio
211 of ghost to all intact cells 0.37% (n_{intact} = 2439 and n_{ghost} = 9) (Fig. 4H and I), similar to
212 the ghosts constructed by Triton X-100 containing 1 mM ATP + 0.01 mM ADP.
213 However, only 33.3% of ghosts continued to glide for 17 min of video recording under
214 ATP + V_i conditions, which is half of the ghosts constructed by Triton X-100 containing

bioRxiv preprint doi: https://doi.org/10.1101/620922; this version posted April 28, 2019. The copyright holder for this preprint (which was not certified by peer review) is the author/funder, who has granted bioRxiv a license to display the preprint in perpetuity. It is made available under aCC-BY-NC-ND 4.0 International license.

215 1 mM ATP + 0.01 mM ADP (Fig. 4J), suggesting that V_i gradually stopped the gliding
216 of ghosts. These results indicate that the gliding motility of *M. gallisepticum* is driven
217 by ATP hydrolysis.

218 **Damage to cell membranes by treatment with Triton X-100**

219 Cells treated with 0.007% Triton X-100 became round and showed three levels of
220 cell-image density shifts (Fig. 4D and E; see Fig. S5 in the supplemental material).
221 Negative-staining electron microscopy was carried out to analyze the morphological
222 changes and cell-image density shifts in detail. Intact cells showed a pear-shape with a
223 membrane protrusion called a 'bleb' and 'infrableb,' as previously reported (Fig. 5A)(37,
224 49). Cells treated with Triton X-100 solution containing 1 mM ATP + 0.01 mM ADP
225 showed a round cell shape (Fig. 5B), consistent with our observations by optical
226 microscopy. Some of the cells had large or small holes on the cell membrane (Fig. 5C–
227 E). These results indicate that the cells treated with Triton X-100 solution have a
228 permeabilized membrane causing the loss of cytoplasm.

229

230 **DISCUSSION**

231 **Gliding behaviors**

232 In the present study, we observed and analyzed the gliding behaviors of *M.*

bioRxiv preprint doi: https://doi.org/10.1101/620922; this version posted April 28, 2019. The copyright holder for this preprint (which was not certified by peer review) is the author/funder, who has granted bioRxiv a license to display the preprint in perpetuity. It is made available under aCC-BY-NC-ND 4.0 International license.

233 *gallisepticum* by using optical microscopes. The gliding speed of *M. gallisepticum*
234 measured in the present study was about 0.27 μm/s (Fig. 1C), which is comparable to
235 the reported gliding speeds of *M. pneumoniae* and *M. genitalium*, about 0.64 μm/s and
236 0.15 μm/s, respectively (39). A previous study shows that *M. genitalium* has curved
237 attachment organelles and a circular trajectory of gliding, but the deletion mutant of
238 MG_217 protein shows straight attachment organelles and a straight trajectory,
239 suggesting that the gliding direction is determined by the alignment of the attachment
240 organelle (23). *M. gallisepticum* has non-bended attachment organelles (Fig. 5A) (37),
241 and the average gliding direction was 0.6 ± 44.6 degrees/5 s (Fig. 1D), which is
242 consistent with previous observations (23, 41). However, cells sometimes glided to the
243 left or the right (Fig. 1B). In these cases, the cells bind to glass surfaces at the end of the
244 membrane protrusion so that the thermal fluctuations and drag of the cell body likely
245 changes the gliding direction to left or right.
246 *M. gallisepticum* did not roll around the cell axis during gliding (Fig. 1E; see Fig. S1 in
247 the supplemental material). Previous studies show that *M. mobile* does not roll even
248 with adhesin complexes working as a 'leg' around the membrane protrusion (41, 50, 51).
249 *M. gallisepticum* and *M. mobile* glide on the ciliated epithelial cells of birds and the gills
250 of fresh-water fish in nature, respectively. The distribution of adhesin complexes may be

bioRxiv preprint doi: https://doi.org/10.1101/620922; this version posted April 28, 2019. The copyright holder for this preprint (which was not certified by peer review) is the author/funder, who has granted bioRxiv a license to display the preprint in perpetuity. It is made available under aCC-BY-NC-ND 4.0 International license.

an advantage for binding to host surfaces because these tissue surfaces are three-dimensionally aligned.

Different inhibitory effects of MC and Ficoll on gliding

In this study, it was found that MC and Ficoll have different inhibitory effects on *M. gallisepticum* gliding (Fig. 2). Previous studies show that a periplasmic flagellated bacterium whose flagella are located between the inner and outer membranes, *Brachyspira pilosicoli*, exhibits swimming at a constant speed in various concentrations of polyvinylpyrrolidone. These results show similar characteristics to MC, but the swimming speed decreased with Ficoll concentrations (43). External flagellated bacteria, *Pseudomonas viscosa*, *Bacillus brevis*, and *Escherichia coli*, increased swimming speeds in 1.33 mPa s of MC (52). Magariyama and Kudo suggested in 2002 that a gel-like three-dimensional network formed by MC makes a virtual tube around the cell body, and the body moves easily in the tube (42). This virtual tube may support the gliding motility of *M. gallisepticum*, enabling the cells to glide even in viscous environments constantly.

Cooperativity in binding

Binding and gliding speed sigmoidally decreased by free SL (Fig. 3C and D). Previous studies show that one adhesin complex of *M. pneumoniae* is composed of two

bioRxiv preprint doi: https://doi.org/10.1101/620922; this version posted April 28, 2019. The copyright holder for this preprint (which was not certified by peer review) is the author/funder, who has granted bioRxiv a license to display the preprint in perpetuity. It is made available under aCC-BY-NC-ND 4.0 International license.

heterodimers, one of each is assembled by one P1 adhesin molecule and one P90 molecule (28). The adhesin complex in *M. genitalium* is also composed of a dimer of heterodimers constructed by P110 and P140, the homologs of P1 adhesin and P90, respectively (53). P110 has a binding site for SOs, so one adhesin complex binds two SOs (31). The adhesin complex of *M. gallisepticum* is assumed to have two binding sites for SOs because it is composed of CrmA and GapA, the homologs of P110 and P140, respectively. This assumption is consistent with 1.55 of the Hill constant. The Hill constant of binding between *M. pneumoniae* cells and sialic compounds ranges from 1.5 to 2.5 (45), comparable to 1.55 of the Hill constant for *M. gallisepticum* (see Fig. S3 in the supplemental material).

In 0.5 mM SL conditions, cells rotating around the end of the membrane protrusion were observed (see Fig. S2 in the supplemental material). A previous study shows that the ghosts of *M. mobile* exhibit directed rotational motility around the membrane protrusion driven by the linear motion of the legs (34). In contrast, rotary motion in *M. gallisepticum* seems to be driven by thermal fluctuation because it has no regularity of rotational direction (see Fig. S2 in the supplemental material), suggesting the possibility that adhesin complexes exist with high density at the end of the membrane protrusion.

Energy source

bioRxiv preprint doi: https://doi.org/10.1101/620922; this version posted April 28, 2019. The copyright holder for this preprint (which was not certified by peer review) is the author/funder, who has granted bioRxiv a license to display the preprint in perpetuity. It is made available under aCC-BY-NC-ND 4.0 International license.

287 In the present study, we succeeded in forming the gliding ghosts of *M. gallisepticum* and
288 clarified that the direct energy source of gliding is ATP (Fig. 4). In this method, we
289 added 0.01 mM ADP to 0.007% Triton X-100 and 1 mM ATP solution because cells
290 permeabilized with 0.007% Triton X-100 and 1 mM ATP solution easily detach from
291 glass surfaces and ADP reduces these detachments.
292 In a previous study, the gliding ghosts of *M. mobile* glided at similar speeds to intact
293 cells, and 85% of ghosts showed gliding (32). However, the gliding speed of *M.*
294 *gallisepticum* ghosts was 4% of that of the intact cells, and 0.4% of the intact cells
295 became gliding ghosts (Fig. 4I and J). Kawamoto *et al*. showed in 2016 that the
296 translucent area surrounding the internal core in *M. pneumoniae* might be occupied by
297 less-di□usive materials and play a role in transmitting the movements of the paired
298 plates originating in the bowl complex to the adhesin complexes (7). The low
299 occurrence ratio of gliding ghosts in *M. gallisepticum* may be caused by the
300 permeabilization of cells resulting in the elution of less-di□usive materials. The cells
301 treated with Triton X-100 show three levels of cell-image density shifts (Fig. 4D and E).
302 The cells which decreased in the cell-image density to be 75% of the intact cells
303 probably have permeabilized cell membranes which retain most of the less-di□usive
304 materials.

bioRxiv preprint doi: https://doi.org/10.1101/620922; this version posted April 28, 2019. The copyright holder for this preprint (which was not certified by peer review) is the author/funder, who has granted bioRxiv a license to display the preprint in perpetuity. It is made available under aCC-BY-NC-ND 4.0 International license.

In the gliding motility of *M. mobile*, complexes of MMOBs 1660 and 1670 in internal jellyfish-like structures have been proposed to hydrolyze ATP molecules as a motor (5, 54). Therefore, which proteins work as a motor in the *M. pneumoniae*-type gliding system need to be identified. Fifteen component proteins of the attachment organelles in *M. pneumoniae* have been identified until now (8). One of these proteins has been annotated as Lon, an ATP-dependent protease (8). This protein possibly works as a motor for gliding.

Generally, respirable bacteria generate a proton gradient across the cell membrane in the respiratory process. The proton gradient causes proton motive force which drives F-type ATP synthase and bacterial flagella (55, 56). However, *Mycoplasmas* have no genes for electron transport and synthesize ATP molecules by glycolysis (57). The membrane potential of *M. gallisepticum* was −48 mV, much smaller than that of typical bacteria, which is −150 mV (58-61). Therefore, ATP is more convenient for *Mycoplasmas* for the energy source of gliding motilities rather than proton motive force.

MATERIALS AND METHODS

Cultivation. The *M. gallisepticum* S6 strain was grown in Aluotto medium at 37□, as previously described (37).

bioRxiv preprint doi: https://doi.org/10.1101/620922; this version posted April 28, 2019. The copyright holder for this preprint (which was not certified by peer review) is the author/funder, who has granted bioRxiv a license to display the preprint in perpetuity. It is made available under aCC-BY-NC-ND 4.0 International license.

323 **Observations of gliding behaviors.** The cells were cultured to reach an optical density
324 at 595 nm of around 0.1. The cultured cells were collected by centrifugation at 12,000 ×
325 *g* for 10 min at room temperature (RT) and suspended in PBS consisting of 75 mM
326 sodium phosphate (pH 7.3) and 68 mM NaCl. The cell suspension was centrifuged at
327 12,000 × *g* for 5 min at RT, suspended in PBS containing 10% non-heat-inactivated
328 horse serum (Gibco; Thermo Fisher Scientific, Waltham, MA), poured through a
329 0.45-μm pore size filter and incubated for 15 min at RT. Then, the cell suspension was
330 poured twice more and inserted into a tunnel chamber which was assembled by taping
331 coverslips cleaned with saturated ethanolic KOH and precoated with 100%
332 non-heat-inactivated horse serum for 60 min and 10 mg/ml bovine serum albumin
333 (Sigma-Aldrich, St. Louis, MO) in PBS for 60 min at RT. The tunnel chamber was
334 washed with PBS containing 20 mM glucose, incubated at 37□ on an inverted
335 microscope (IX83; Olympus, Tokyo, Japan) equipped with a thermo plate
336 (MATS-OTOR-MV; Tokai Hit, Shizuoka, Japan) and a lens heater (MATS-LH; Tokai
337 Hit), observed by phase-contrast microscopy at 37□ and recorded with a
338 charge-coupled device (CCD) camera (LRH2500XE-1; DigiMo, Tokyo, Japan). Video
339 data were analyzed by ImageJ 1.43u (http://rsb.info.nih.gov/ij/), as previously described
340 (37, 41).

bioRxiv preprint doi: https://doi.org/10.1101/620922; this version posted April 28, 2019. The copyright holder for this preprint (which was not certified by peer review) is the author/funder, who has granted bioRxiv a license to display the preprint in perpetuity. It is made available under aCC-BY-NC-ND 4.0 International license.

To investigate the effect of viscosity on gliding, the cultured cells were washed with PBS containing 10% non-heat-inactivated horse serum and 0.10%, 0.25%, and 0.50% MC (Methyl Cellulose #400; nacalai tesque, Kyoto, Japan) or 5%, 10%, and 15% Ficoll (M.W. 400,000; nacalai tesque, Kyoto, Japan), poured and incubated. Then, the cell suspension was poured and inserted into a cleaned and precoated tunnel chamber. The tunnel chamber was washed with various concentrations of viscous buffer containing 20 mM glucose, observed by phase-contrast microscopy at 37□ and recorded. The viscosities were measured using dynamic viscoelasticity measuring apparatus (Rheosol-G5000; UBM, Kyoto, Japan) at 37□ as follows: 0.66 mPa s for PBS/G, 2.5, 5.5, 7.3 mPa s for 0.10%, 0.25%, 0.50% MC, 2.3, 3.0, 4.6 mPa s for 5%, 10%, 15% Ficoll.

Cells on the tunnel chamber were treated with various concentrations of 3′-sialyllactose sodium salt (Nagara Science Co., Ltd, Tokyo, Japan) in PBS/G, observed by phase-contrast microscopy at 37□ and recorded to examine the binding features.

The cultured cells were collected, suspended in PBS containing 10 mM Sulfo-NHSLC-LC-Biotin (Thermo Fisher Scientific) and incubated for 15 min at RT to observe cell rolling. The cell suspension was centrifuged, suspended in PBS containing 10% non-heat-inactivated horse serum, poured, and incubated. Then, the cell suspension

bioRxiv preprint doi: https://doi.org/10.1101/620922; this version posted April 28, 2019. The copyright holder for this preprint (which was not certified by peer review) is the author/funder, who has granted bioRxiv a license to display the preprint in perpetuity. It is made available under aCC-BY-NC-ND 4.0 International license.

359 was poured and inserted into a cleaned and precoated tunnel chamber. The tunnel
360 chamber was washed by PBS/G containing streptavidin conjugated 40 nm colloidal gold
361 (Cytodiagnostics, Ontario, Canada), observed by dark-field microscopy using an upright
362 microscope (BX50; Olympus) at 37□ and recorded by a CCD camera (WAT-120N;
363 Watec Co. Ltd., Yamagata, Japan). Video data were analyzed by ImageJ 1.43u and
364 IGOR Pro 6.33J (WaveMetrics, Portland, OR).

365 **Gliding ghost**

366 The cultured cells were collected and suspended in HEPES buffer (10 mM HEPES pH
367 7.4, 100 mM NaCl). The cell suspension was centrifuged, suspended in bufferA, poured,
368 and incubated for 15 min at RT. Then, the cell suspension was poured and inserted into
369 a cleaned and precoated tunnel chamber. The tunnel chamber was washed with bufferA
370 containing 20 mM glucose, observed by phase-contrast microscopy at 37□, and
371 recorded. After 70 s, the buffer was replaced with 0.007% Triton X-100 (MP
372 Biomedicals, Santa Ana, CA) containing 1 mM ATP and 0.01 mM ADP or 0 mM ATP or
373 1 mM ADP or 1 mM ATP and 0.5 mM Na_3VO_4. Video data were analyzed by ImageJ
374 1.43u.

375 **Negative-staining electron microscopy.** The cultured cells were collected, suspended
376 in PBS containing 10% non-heat-inactivated horse serum, poured through a 0.45-μm

bioRxiv preprint doi: https://doi.org/10.1101/620922; this version posted April 28, 2019. The copyright holder for this preprint (which was not certified by peer review) is the author/funder, who has granted bioRxiv a license to display the preprint in perpetuity. It is made available under aCC-BY-NC-ND 4.0 International license.

pore size filter and incubated for 15 min at RT. Then, the cell suspension was placed on a carbon-coated grid and incubated for 10 min at RT. The grid was treated with 0.007% Triton X-100 containing 1 mM ATP and 0.01 mM ADP to permeabilize cells, incubated for 1 min at RT and fixed with 1% glutaraldehyde in bufferA for 1 min at RT. The fixed cells were washed with water, stained with 0.5% ammonium molybdate, and observed using a transmission electron microscope (JEM-1010; JEOL, Tokyo, Japan) at 80 kV equipped with a CCD camera (FastScan-F214 (T); TVIPS, Gauting, Germany).

ACKNOWLEDGMENTS

We thank Yuhei O Tahara at Osaka City University for technical assistance with negative-staining electron microscopy. This work was supported by a Grant-in-Aid for Scientific Research in the innovative area of ‘’Harmonized Supramolecular Motility Machinery and Its Diversity’ (Ministry of Education, Culture, Sports, Science, and Technology KAKENHI; grant number 24117002) and by a Grants-in-Aid for Scientific Research (A) (Ministry of Education, Culture, Sports, Science, and Technology KAKENHI; grant number 17H01544) to M. Miyata. M. Mizutani is the recipient of a Research Fellowship of the Japan Society for the Promotion of Science (18J15362).

bioRxiv preprint doi: https://doi.org/10.1101/620922; this version posted April 28, 2019. The copyright holder for this preprint (which was not certified by peer review) is the author/funder, who has granted bioRxiv a license to display the preprint in perpetuity. It is made available under aCC-BY-NC-ND 4.0 International license.

REFERENCES

1. Razin S, Yogev D, Naot Y. 1998. Molecular biology and pathogenicity of mycoplasmas. Microbiol Mol Biol Rev 62:1094-156.
2. Razin S, Hayflick L. 2010. Highlights of mycoplasma research--an historical perspective. Biologicals 38:183-90.
3. Miyata M. 2008. Centipede and inchworm models to explain *Mycoplasma* gliding. Trends Microbiol 16:6-12.
4. Miyata M. 2010. Unique centipede mechanism of *Mycoplasma* gliding. Annu Rev Microbiol 64:519-37.
5. Miyata M, Hamaguchi T. 2016. Prospects for the gliding mechanism of *Mycoplasma mobile*. Curr Opin Microbiol 29:15-21.
6. Nakane D, Kenri T, Matsuo L, Miyata M. 2015. Systematic structural analyses of attachment organelle in *Mycoplasma pneumoniae*. PLoS Pathog 11:e1005299.
7. Kawamoto A, Matsuo L, Kato T, Yamamoto H, Namba K, Miyata M. 2016. Periodicity in attachment organelle revealed by electron cryotomography suggests conformational changes in gliding mechanism of *Mycoplasma pneumoniae*. MBio 7:e00243-16.
8. Miyata M, Hamaguchi T. 2016. Integrated information and prospects for gliding

bioRxiv preprint doi: https://doi.org/10.1101/620922; this version posted April 28, 2019. The copyright holder for this preprint (which was not certified by peer review) is the author/funder, who has granted bioRxiv a license to display the preprint in perpetuity. It is made available under aCC-BY-NC-ND 4.0 International license.

413 mechanism of the pathogenic bacterium *Mycoplasma pneumoniae*. Front Microbiol
414 7:960.
415 9. Dandekar T, Huynen M, Regula JT, Ueberle B, Zimmermann CU, Andrade MA,
416 Doerks T, Sanchez-Pulido L, Snel B, Suyama M, Yuan YP, Herrmann R, Bork P.
417 2000. Re-annotating the *Mycoplasma pneumoniae* genome sequence: adding value,
418 function and reading frames. Nucleic Acids Res 28:3278-88.
419 10. Jaffe JD, Stange-Thomann N, Smith C, DeCaprio D, Fisher S, Butler J, Calvo S,
420 Elkins T, FitzGerald MG, Hafez N, Kodira CD, Major J, Wang S, Wilkinson J,
421 Nicol R, Nusbaum C, Birren B, Berg HC, Church GM. 2004. The complete genome
422 and proteome of *Mycoplasma mobile*. Genome Res 14:1447-61.
423 11. Seybert A, Gonzalez-Gonzalez L, Scheffer MP, Lluch-Senar M, Mariscal AM,
424 Querol E, Matthaeus F, Pinol J, Frangakis AS. 2018. Cryo-electron tomography
425 analyses of terminal organelle mutants suggest the motility mechanism of
426 *Mycoplasma genitalium*. Mol Microbiol 108:319-329.
427 12. Meng KE, Pfister RM. 1980. Intracellular structures of *Mycoplasma pneumoniae*
428 revealed after membrane removal. J Bacteriol 144:390-9.
429 13. Henderson GP, Jensen GJ. 2006. Three-dimensional structure of *Mycoplasma*
430 *pneumoniae*'s attachment organelle and a model for its role in gliding motility. Mol

bioRxiv preprint doi: https://doi.org/10.1101/620922; this version posted April 28, 2019. The copyright holder for this preprint (which was not certified by peer review) is the author/funder, who has granted bioRxiv a license to display the preprint in perpetuity. It is made available under aCC-BY-NC-ND 4.0 International license.

Microbiol 60:376-85.

14. Seybert A, Herrmann R, Frangakis AS. 2006. Structural analysis of *Mycoplasma pneumoniae* by cryo-electron tomography. J Struct Biol 156:342-54.

15. Hegermann J, Herrmann R, Mayer F. 2002. Cytoskeletal elements in the bacterium *Mycoplasma pneumoniae*. Naturwissenschaften 89:453-8.

16. Pich OQ, Burgos R, Ferrer-Navarro M, Querol E, Pinol J. 2006. *Mycoplasma genitalium mg200* and *mg386* genes are involved in gliding motility but not in cytadherence. Mol Microbiol 60:1509-19.

17. Jordan JL, Chang HY, Balish MF, Holt LS, Bose SR, Hasselbring BM, Waldo RH, 3rd, Krunkosky TM, Krause DC. 2007. Protein P200 is dispensable for *Mycoplasma pneumoniae* hemadsorption but not gliding motility or colonization of differentiated bronchial epithelium. Infect Immun 75:518-22.

18. Popham PL, Hahn TW, Krebes KA, Krause DC. 1997. Loss of HMW1 and HMW3 in noncytadhering mutants of *Mycoplasma pneumoniae* occurs post-translationally. Proc Natl Acad Sci U S A 94:13979-84.

19. Hahn TW, Willby MJ, Krause DC. 1998. HMW1 is required for cytadhesin P1 trafficking to the attachment organelle in *Mycoplasma pneumoniae*. J Bacteriol 180:1270-6.

bioRxiv preprint doi: https://doi.org/10.1101/620922; this version posted April 28, 2019. The copyright holder for this preprint (which was not certified by peer review) is the author/funder, who has granted bioRxiv a license to display the preprint in perpetuity. It is made available under aCC-BY-NC-ND 4.0 International license.

449 20. Seto S, Miyata M. 2003. Attachment organelle formation represented by
450 localization of cytadherence proteins and formation of the electron-dense core in
451 wild-type and mutant strains of *Mycoplasma pneumoniae*. J Bacteriol 185:1082-91.
452 21. Kenri T, Seto S, Horino A, Sasaki Y, Sasaki T, Miyata M. 2004. Use of
453 fluorescent-protein tagging to determine the subcellular localization of *Mycoplasma*
454 *pneumoniae* proteins encoded by the cytadherence regulatory locus. J Bacteriol
455 186:6944-55.
456 22. Burgos R, Pich OQ, Querol E, Pinol J. 2007. Functional analysis of the
457 *Mycoplasma genitalium* MG312 protein reveals a specific requirement of the
458 MG312 N-terminal domain for gliding motility. J Bacteriol 189:7014-23.
459 23. Burgos R, Pich OQ, Querol E, Pinol J. 2008. Deletion of the *Mycoplasma*
460 *genitalium* MG_217 gene modifies cell gliding behaviour by altering terminal
461 organelle curvature. Mol Microbiol 69:1029-40.
462 24. Bose SR, Balish MF, Krause DC. 2009. *Mycoplasma pneumoniae* cytoskeletal
463 protein HMW2 and the architecture of the terminal organelle. J Bacteriol
464 191:6741-8.
465 25. Jordan JL, Berry KM, Balish MF, Krause DC. 2001. Stability and subcellular
466 localization of cytadherence-associated protein P65 in *Mycoplasma pneumoniae*. J

bioRxiv preprint doi: https://doi.org/10.1101/620922; this version posted April 28, 2019. The copyright holder for this preprint (which was not certified by peer review) is the author/funder, who has granted bioRxiv a license to display the preprint in perpetuity. It is made available under aCC-BY-NC-ND 4.0 International license.

467 Bacteriol 183:7387-91.

468 26. Chang HY, Prince OA, Sheppard ES, Krause DC. 2011. Processing is required for a

469 fully functional protein P30 in *Mycoplasma pneumoniae* gliding and cytadherence.

470 J Bacteriol 193:5841-6.

471 27. Hasselbring BM, Sheppard ES, Krause DC. 2012. P65 truncation impacts P30

472 dynamics during *Mycoplasma pneumoniae* gliding. J Bacteriol 194:3000-7.

473 28. Nakane D, Adan-Kubo J, Kenri T, Miyata M. 2011. Isolation and characterization

474 of P1 adhesin, a leg protein of the gliding bacterium *Mycoplasma pneumoniae*. J

475 Bacteriol 193:715-22.

476 29. Layh-Schmitt G, Herrmann R. 1992. Localization and biochemical characterization

477 of the ORF6 gene product of the *Mycoplasma pneumoniae* P1 operon. Infect

478 Immun 60:2906-13.

479 30. Catrein I, Herrmann R, Bosserhoff A, Ruppert T. 2005. Experimental proof for a

480 signal peptidase I like activity in *Mycoplasma pneumoniae*, but absence of a gene

481 encoding a conserved bacterial type I SPase. FEBS J 272:2892-900.

482 31. Aparicio D, Torres-Puig S, Ratera M, Querol E, Pinol J, Pich OQ, Fita I. 2018.

483 *Mycoplasma genitalium* adhesin P110 binds sialic-acid human receptors. Nat

484 Commun 9:4471.

bioRxiv preprint doi: https://doi.org/10.1101/620922; this version posted April 28, 2019. The copyright holder for this preprint (which was not certified by peer review) is the author/funder, who has granted bioRxiv a license to display the preprint in perpetuity. It is made available under aCC-BY-NC-ND 4.0 International license.

485 32. Uenoyama A, Miyata M. 2005. Gliding ghosts of *Mycoplasma mobile*. Proc Natl
486 Acad Sci USA 102:12754-8.
487 33. Kinosita Y, Nakane D, Sugawa M, Masaike T, Mizutani K, Miyata M, Nishizaka T.
488 2014. Unitary step of gliding machinery in *Mycoplasma mobile*. Proc Natl Acad Sci
489 USA 111:8601-6.
490 34. Kinosita Y, Miyata M, Nishizaka T. 2018. Linear motor driven-rotary motion of a
491 membrane-permeabilized ghost in *Mycoplasma mobile*. Sci Rep 8:11513.
492 35. Levisohn S, Kleven SH. 2000. Avian mycoplasmosis (*Mycoplasma gallisepticum*).
493 Rev Sci Tech 19:425-42.
494 36. Indikova I, Vronka M, Szostak MP. 2014. First identification of proteins involved in
495 motility of *Mycoplasma gallisepticum*. Vet Res 45:99.
496 37. Nakane D, Miyata M. 2009. Cytoskeletal asymmetrical dumbbell structure of a
497 gliding mycoplasma, *Mycoplasma gallisepticum*, revealed by negative-staining
498 electron microscopy. J Bacteriol 191:3256-64.
499 38. Indikova I, Much P, Stipkovits L, Siebert-Gulle K, Szostak MP, Rosengarten R,
500 Citti C. 2013. Role of the GapA and CrmA cytadhesins of *Mycoplasma*
501 *gallisepticum* in promoting virulence and host colonization. Infect Immun
502 81:1618-24.

bioRxiv preprint doi: https://doi.org/10.1101/620922; this version posted April 28, 2019. The copyright holder for this preprint (which was not certified by peer review) is the author/funder, who has granted bioRxiv a license to display the preprint in perpetuity. It is made available under aCC-BY-NC-ND 4.0 International license.

503 39. Miyata M, Nakane D. 2013. Gliding mechanism of the *Mycoplasma pneumoniae*
504 subgroup implications from studies on *Mycoplasma mobile*. in Molecular and Cell
505 Biology of Mollicutes, eds G Browning and C Citti (Norfolk: Horizon
506 Press):237–252.
507 40. Erdmann T. 1976. Untersuchungen zur morphologie, vermehrung und
508 beweglichkeit von *Mycoplasma gallisepticum*. MD thesis Johannes Gutenberg
509 Universita¨t, Mainz, Germany.
510 41. Morio H, Kasai T, Miyata M. 2016. Gliding direction of *Mycoplasma mobile*. J
511 Bacteriol 198:283-90.
512 42. Magariyama Y, Kudo S. 2002. A mathematical explanation of an increase in
513 bacterial swimming speed with viscosity in linear-polymer solutions. Biophys J
514 83:733-9.
515 43. Nakamura S, Adachi Y, Goto T, Magariyama Y. 2006. Improvement in motion
516 efficiency of the spirochete *Brachyspira pilosicoli* in viscous environments.
517 Biophys J 90:3019-26.
518 44. Nagai R, Miyata M. 2006. Gliding motility of *Mycoplasma mobile* can occur by
519 repeated binding to *N*-acetylneuraminyllactose (sialyllactose) fixed on solid
520 surfaces. J Bacteriol 188:6469-75.

bioRxiv preprint doi: https://doi.org/10.1101/620922; this version posted April 28, 2019. The copyright holder for this preprint (which was not certified by peer review) is the author/funder, who has granted bioRxiv a license to display the preprint in perpetuity. It is made available under aCC-BY-NC-ND 4.0 International license.

521 45. Kasai T, Nakane D, Ishida H, Ando H, Kiso M, Miyata M. 2013. Role of binding in
522 *Mycoplasma mobile* and *Mycoplasma pneumoniae* gliding analyzed through
523 inhibition by synthesized sialylated compounds. J Bacteriol 195:429-35.
524 46. Mizutani M, Tulum I, Kinosita Y, Nishizaka T, Miyata M. 2018. Detailed analyses
525 of stall force generation in *Mycoplasma mobile* gliding. Biophys J 114:1411-1419.
526 47. Shimizu T, Johnson KA. 1983. Presteady state kinetic analysis of vanadate-induced
527 inhibition of the dynein ATPase. J Biol Chem 258:13833-40.
528 48. Burgess SA, Walker ML, Sakakibara H, Knight PJ, Oiwa K. 2003. Dynein structure
529 and power stroke. Nature 421:715-8.
530 49. Maniloff J, Morowitz HJ, Barrnett RJ. 1965. Ultrastructure and Ribosomes of
531 *Mycoplasma gallisepticum*. J Bacteriol 90:193-204.
532 50. Miyata M, Uenoyama A. 2002. Movement on the cell surface of the gliding
533 bacterium, *Mycoplasma mobile*, is limited to its head-like structure. FEMS
534 Microbiol Lett 215:285-9.
535 51. Uenoyama A, Kusumoto A, Miyata M. 2004. Identification of a 349-kilodalton
536 protein (Gli349) responsible for cytadherence and glass binding during gliding of
537 *Mycoplasma mobile*. J Bacteriol 186:1537-45.
538 52. Shoesmith JH, Sherris JC. 1960. Studies on the mechanism of arginine-activated

bioRxiv preprint doi: https://doi.org/10.1101/620922; this version posted April 28, 2019. The copyright holder for this preprint (which was not certified by peer review) is the author/funder, who has granted bioRxiv a license to display the preprint in perpetuity. It is made available under aCC-BY-NC-ND 4.0 International license.

motility in a *Pseudomonas* strain. J Gen Microbiol 22:10-24.

53. Scheffer MP, Gonzalez-Gonzalez L, Seybert A, Ratera M, Kunz M, Valpuesta JM, Fita I, Querol E, Pinol J, Martin-Benito J, Frangakis AS. 2017. Structural characterization of the NAP; the major adhesion complex of the human pathogen *Mycoplasma genitalium*. Mol Microbiol 105:869-879.

54. Nakane D, Miyata M. 2007. Cytoskeletal "Jellyfish" structure of *Mycoplasma mobile*. Proc Natl Acad Sci USA 104:19518-19523.

55. Berg HC. 2003. The rotary motor of bacterial flagella. Annu Rev Biochem 72:19-54.

56. Noji H, Ueno H, McMillan DGG. 2017. Catalytic robustness and torque generation of the F_1-ATPase. Biophys Rev 9:103-118.

57. Fraser CM, Gocayne JD, White O, Adams MD, Clayton RA, Fleischmann RD, Bult CJ, Kerlavage AR, Sutton G, Kelley JM, Fritchman RD, Weidman JF, Small KV, Sandusky M, Fuhrmann J, Nguyen D, Utterback TR, Saudek DM, Phillips CA, Merrick JM, Tomb JF, Dougherty BA, Bott KF, Hu PC, Lucier TS, Peterson SN, Smith HO, Hutchison CA, 3rd, Venter JC. 1995. The minimal gene complement of *Mycoplasma genitalium*. Science 270:397-403.

58. Griniuviene B, Chmieliauskaite V, Grinius L. 1974. Energy-linked transport of

bioRxiv preprint doi: https://doi.org/10.1101/620922; this version posted April 28, 2019. The copyright holder for this preprint (which was not certified by peer review) is the author/funder, who has granted bioRxiv a license to display the preprint in perpetuity. It is made available under aCC-BY-NC-ND 4.0 International license.

permeant ions in *Escherichia coli* cells: evidence for membrane potential generation by proton-pump. Biochem Biophys Res Commun 56:206-13.

59. Mates SM, Eisenberg ES, Mandel LJ, Patel L, Kaback HR, Miller MH. 1982. Membrane potential and gentamicin uptake in *Staphylococcus aureus*. Proc Natl Acad Sci U S A 79:6693-7.

60. Schiefer HG, Schummer U. 1982. The electrochemical potential across mycoplasmal membranes. Rev Infect Dis 4 Suppl: S65-70.

61. Lo CJ, Leake MC, Pilizota T, Berry RM. 2007. Nonequivalence of membrane voltage and ion-gradient as driving forces for the bacterial flagellar motor at low load. Biophys J 93:294-302.

bioRxiv preprint doi: https://doi.org/10.1101/620922; this version posted April 28, 2019. The copyright holder for this preprint (which was not certified by peer review) is the author/funder, who has granted bioRxiv a license to display the preprint in perpetuity. It is made available under aCC-BY-NC-ND 4.0 International license.

569 **Figures**

570 Fig. 1 Gliding behaviors.

571 (A) Phase-contrast micrograph of *M. gallisepticum* cells. The cells on the glass are

572 gliding in the direction of the membrane protrusion marked by white triangles. (B) Field

573 image of phase-contrast micrograph (left) and cell trajectories for 30 s, changing color

574 with time from red to blue (right). (C) Distribution of gliding speeds averaged for 60 s

575 at 1 s intervals was fitted with a Gaussian curve (n = 231). (D) Schematic illustration

576 showing the measurement of gliding direction (left) and the distribution of gliding

577 directions (right). Five consecutive cell images at 5 s intervals are shown in the same

578 field. The cell axis and gliding directions are shown by black lines and yellow sectors,

579 respectively. The cell glided in the direction indicated by the black arrow (left). The

580 distribution was fitted with a Gaussian curve (right). (E) Dark-field micrograph of a cell

581 attached with colloidal gold (left) and trajectories (right). Four consecutive images of a

582 cell attached with colloidal gold at 10 s intervals are shown in the same field. The cell

583 glided in the direction indicated by the white arrow (left). The trajectories of the mass

584 centers of the cell and colloidal gold are indicated by black and red lines, respectively

585 (right).

bioRxiv preprint doi: https://doi.org/10.1101/620922; this version posted April 28, 2019. The copyright holder for this preprint (which was not certified by peer review) is the author/funder, who has granted bioRxiv a license to display the preprint in perpetuity. It is made available under aCC-BY-NC-ND 4.0 International license.

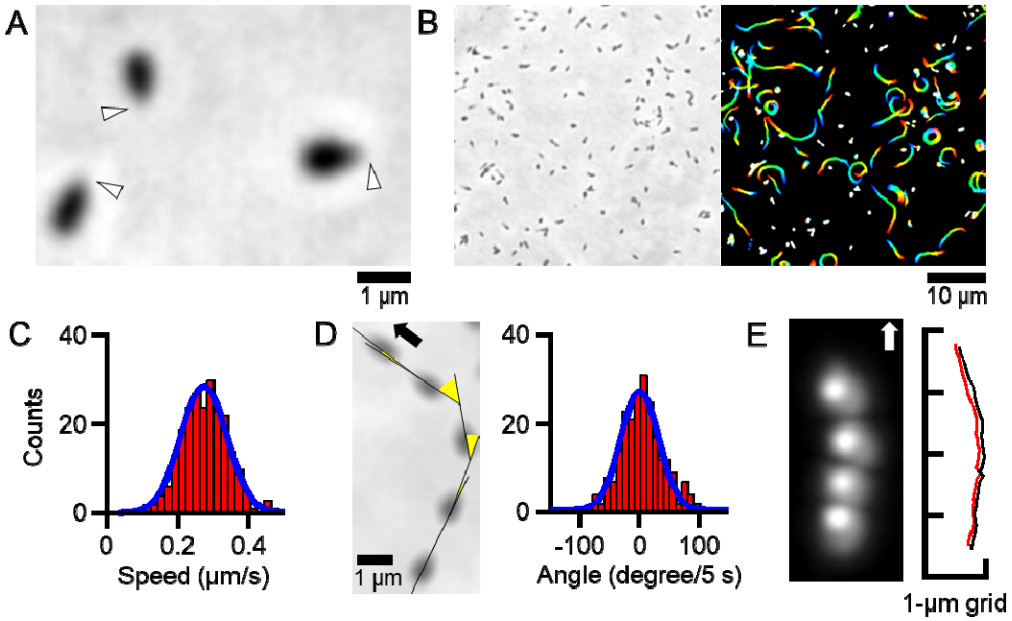

586

587

bioRxiv preprint doi: https://doi.org/10.1101/620922; this version posted April 28, 2019. The copyright holder for this preprint (which was not certified by peer review) is the author/funder, who has granted bioRxiv a license to display the preprint in perpetuity. It is made available under aCC-BY-NC-ND 4.0 International license.

588 Fig. 2 Effects of MC and Ficoll on gliding.

589 (A) Cell trajectories for 60 s under PBS/G (top), 0.50% MC (middle) and 15% Ficoll

590 (bottom). The color changes with time from red to blue. (B) Distributions of gliding

591 speeds and directions under PBS/G (top), PBS/G containing 0.5% MC (middle) and

592 15% Ficoll (bottom) were fitted with Gaussian curves. (C) Gliding speeds and

593 directions under various concentrations of MC or Ficoll. The average gliding speeds for

594 60 s at 1 s intervals and the average gliding directions every 5 s for 60 s under PBS/G

595 containing 0%, 0.10%, 0.25%, 0.50% MC or 5%, 10%, 15% Ficoll conditions are

596 plotted with standard deviations. Black, red, and blue circles indicate PBS/G, MC, and

597 Ficoll, respectively.

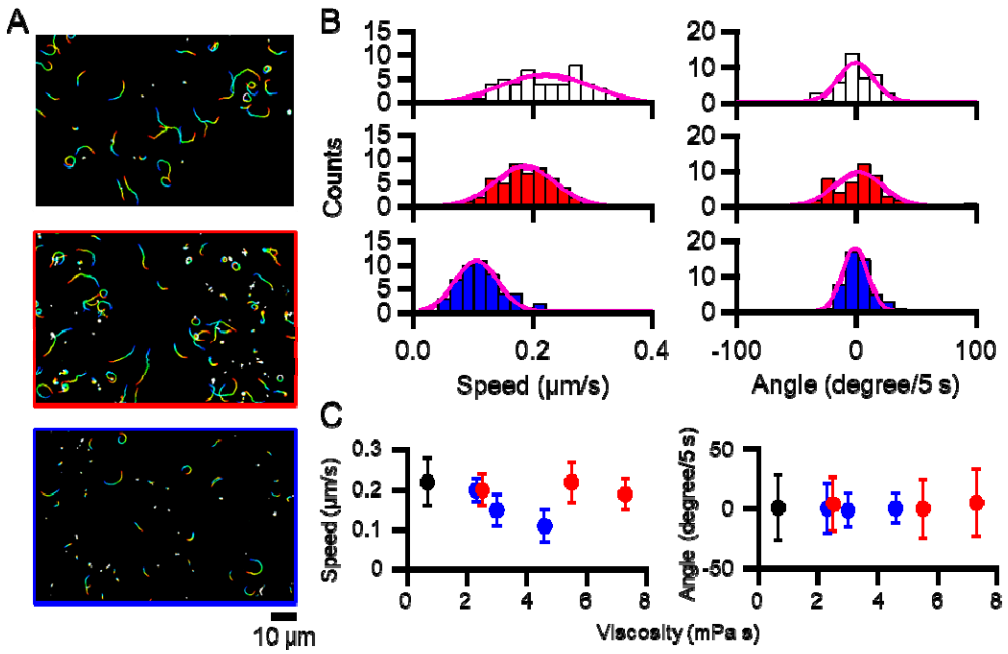

598

599

bioRxiv preprint doi: https://doi.org/10.1101/620922; this version posted April 28, 2019. The copyright holder for this preprint (which was not certified by peer review) is the author/funder, who has granted bioRxiv a license to display the preprint in perpetuity. It is made available under aCC-BY-NC-ND 4.0 International license.

Fig. 3 Effects of SL on binding and gliding

(A) Cell trajectories for 60 s under various concentrations of SL. The color changes with time from red to blue. (B) Changes in gliding speeds by the addition of SL. Dotted lines indicate the time point when various concentrations of SL were added. The gliding speeds of individual cells are plotted as dots for every 10 s. (n_{cells} = 9, 9, 10, 6, 6, 9 for 0, 0.1, 0.2, 0.3, 0.4, 0.5 mM SL, respectively). The average gliding speeds are shown with solid lines. The gliding speeds from 0 to 10 s in each condition are normalized as 100%. (C) The gliding cell ratios under each SL concentration are plotted with standard deviations and fitted with a sigmoidal curve. (D) The gliding speeds under each SL concentration are plotted with standard deviations and fitted with a sigmoidal curve.

bioRxiv preprint doi: https://doi.org/10.1101/620922; this version posted April 28, 2019. The copyright holder for this preprint (which was not certified by peer review) is the author/funder, who has granted bioRxiv a license to display the preprint in perpetuity. It is made available under aCC-BY-NC-ND 4.0 International license.

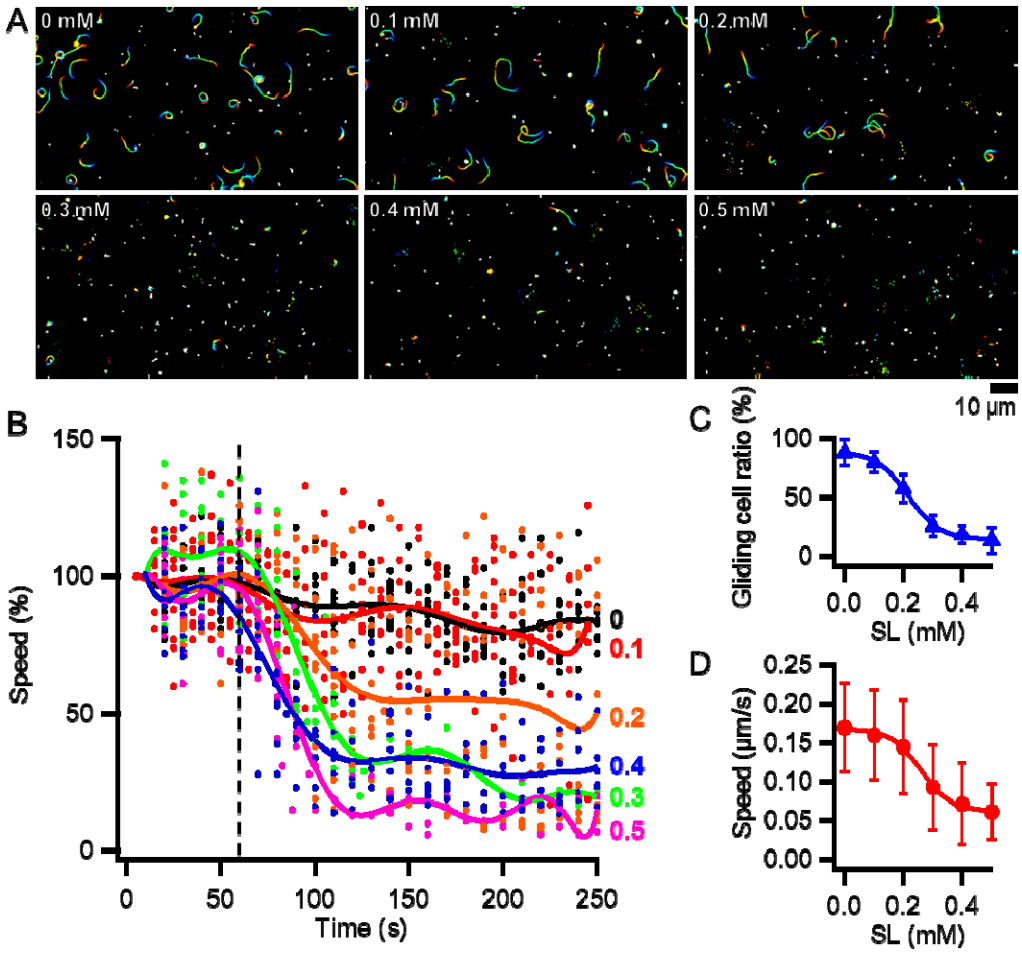

610

611

bioRxiv preprint doi: https://doi.org/10.1101/620922; this version posted April 28, 2019. The copyright holder for this preprint (which was not certified by peer review) is the author/funder, who has granted bioRxiv a license to display the preprint in perpetuity. It is made available under aCC-BY-NC-ND 4.0 International license.

612 Fig. 4 Gliding ghost

613 (A) Trajectories for 250 s at 5 s intervals of all cells (left) and the cell to be the gliding
614 ghost (right). The color changes with time from red to blue. The 0.007% Triton X-100
615 containing 1 mM ATP + 0.01 mM ADP solution was added at 0 s. (B) Phase-contrast
616 micrographs of intact (upper), pre-permeabilized (middle) and post-permeabilized cells
617 (lower) marked with white triangles in (A). The time points after the addition of Triton
618 solutions are shown in each panel. (C) Transitions of gliding speeds and cell-image
619 densities. The average gliding speeds and cell-image densities for 10 s at 1-s intervals
620 are plotted as black circles and gray triangles, respectively. The average cell-image
621 densities from -60 to -50 s is normalized as 100%. ‘Tri’ and ‘Per’ indicate the time
622 points when 0.007% Triton X-100 containing 1 mM ATP + 0.01 mM ADP solution was
623 added, and the density shift occurred, respectively. (D) The phase-contrast micrograph
624 of cells treated with Triton solution. Cells showed three levels of cell-image density
625 shifts; the image density did not decrease (right-upper), the image density decreased to
626 be about 75% of the intact cell (left-upper), and the image density decreased to half of
627 the intact cell (left-lower). (E) Distribution of cell-image densities at 90 s after the
628 addition of Triton solution was fitted by the sum of three Gaussian curves. The
629 individual Gaussian curves and the sum of three Gaussian curves are indicated by black

bioRxiv preprint doi: https://doi.org/10.1101/620922; this version posted April 28, 2019. The copyright holder for this preprint (which was not certified by peer review) is the author/funder, who has granted bioRxiv a license to display the preprint in perpetuity. It is made available under aCC-BY-NC-ND 4.0 International license.

broken and magenta solid lines, respectively. The cell-image density before Triton treatment is normalized as 100%. The positions of peak tops are indicated by black triangles. (F) Ghosts constructed by Triton X-100 solutions including nucleotides. Intact, pre-permeabilized, post-permeabilized, and trajectories of ghosts for 15 min are shown from left to right panels. The color changes with time from red to blue. The time points after the addition of Triton solutions are shown in each panel. The cells indicated by black circles decrease for the cell-image densities to be about 75% at post-permeabilized panels. (G) Distribution of gliding speeds of ghosts constructed by 0.007% Triton X-100 containing 1 mM ATP + 0.01 mM ADP solution fitted with a Gaussian curve. (H) The average gliding speeds of ghosts constructed with Triton X-100 solution including ATP or ATP-V_i are shown with standard deviations. (I) The occurrence ratios of gliding ghosts to all intact cells are shown. (J) The ratios of ghosts which continued to glide through 17 min of video recording are shown.

bioRxiv preprint doi: https://doi.org/10.1101/620922; this version posted April 28, 2019. The copyright holder for this preprint (which was not certified by peer review) is the author/funder, who has granted bioRxiv a license to display the preprint in perpetuity. It is made available under aCC-BY-NC-ND 4.0 International license.

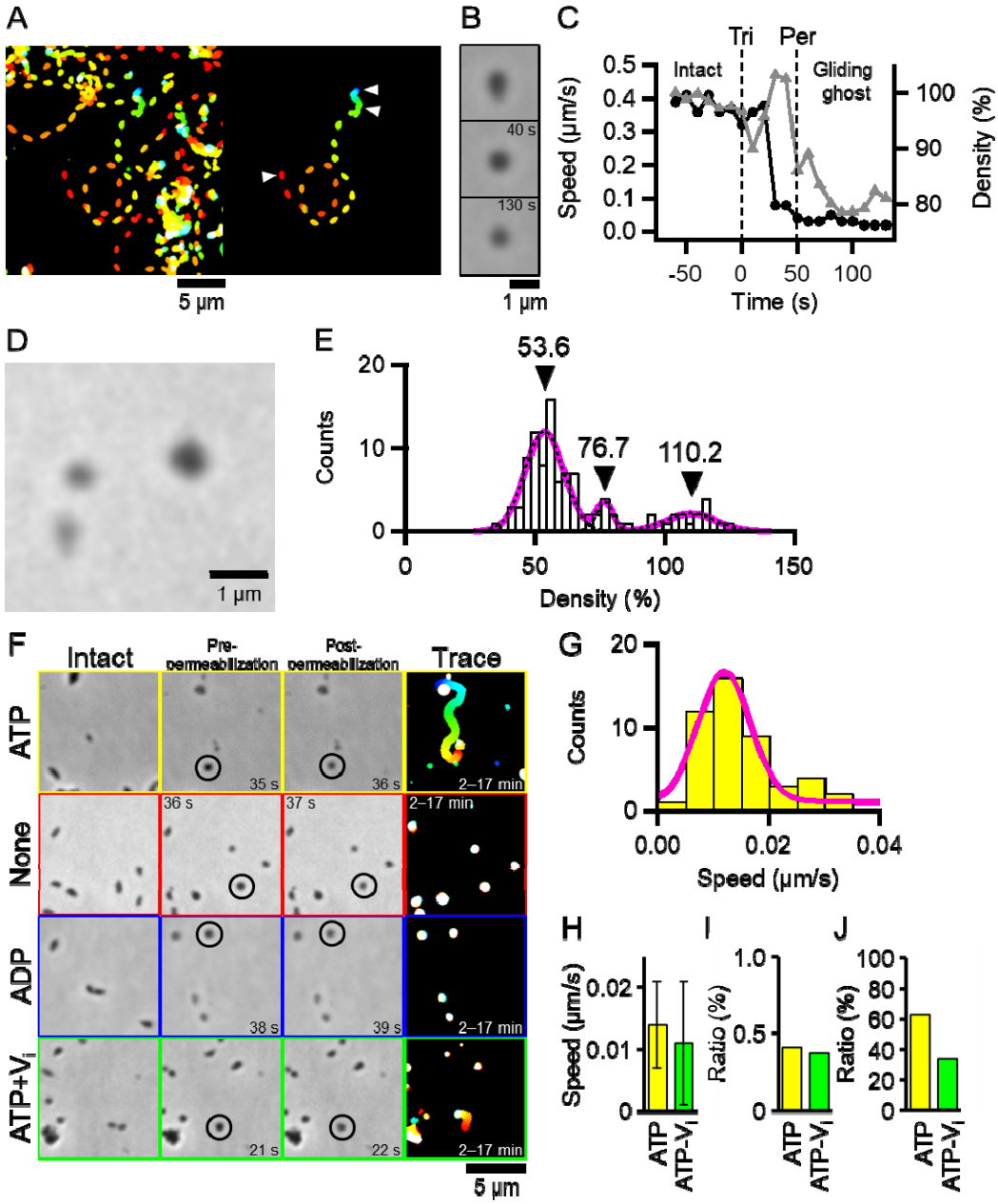

643

644

bioRxiv preprint doi: https://doi.org/10.1101/620922; this version posted April 28, 2019. The copyright holder for this preprint (which was not certified by peer review) is the author/funder, who has granted bioRxiv a license to display the preprint in perpetuity. It is made available under aCC-BY-NC-ND 4.0 International license.

645 Fig. 5 Negative-staining electron micrographs of cell permeabilization.

646 (A) Intact cells. The cells featured by the bleb and infrableb are shown. (B–E) Cells

647 treated with 0.007% Triton X-100 containing 1 mM ATP + 0.01 mM ADP. Some of the

648 permeabilized cells have large (C) or small (D) holes marked by yellow triangles. (E)

649 Magnified images of red boxed areas in (D). A–D show the same magnification. Two

650 examples of images are shown for each category.

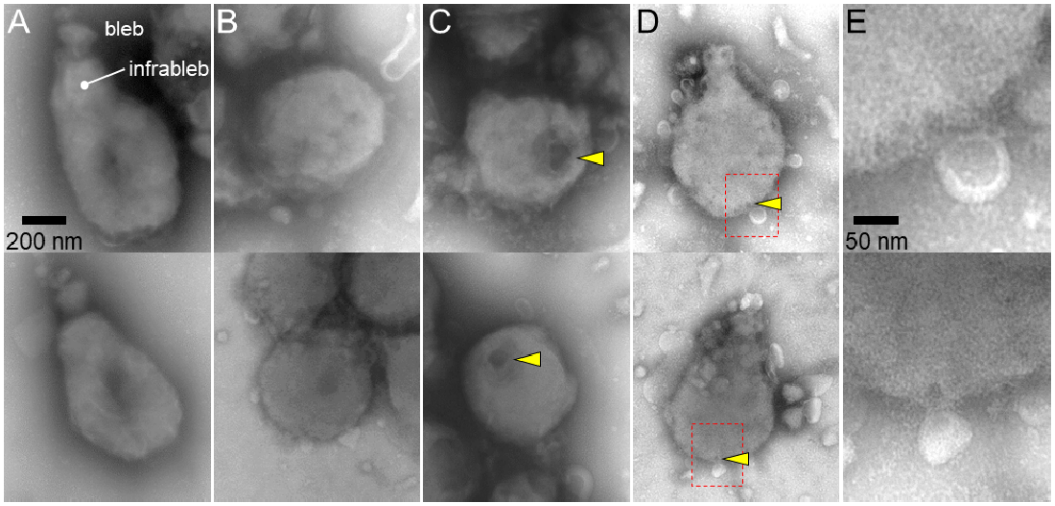

651

652

653

bioRxiv preprint doi: https://doi.org/10.1101/620922; this version posted April 28, 2019. The copyright holder for this preprint (which was not certified by peer review) is the author/funder, who has granted bioRxiv a license to display the preprint in perpetuity. It is made available under aCC-BY-NC-ND 4.0 International license.

654 Fig. S1 Gliding motility of cells attached with colloidal gold.

655 (A) The field image of dark-field microscopy. The yellow triangles indicate the

656 examples of colloidal gold attached to cells. (left). The cell trajectories for 60 s,

657 changing color with time from red to blue (right). (B) The distributions of gliding

658 speeds with (upper) and without colloidal gold (lower). The averaged gliding speeds

659 with standard deviations are shown in each panel. (C). Four consecutive dark-field

660 micrographs of a cell attached with a colloidal gold at 20 s intervals are shown in the

661 same field. The cell glided in the direction indicated by a white arrow. These

662 micrographs are shown in scale with (D). (D) The trajectories of the mass centers of

663 cells and colloidal gold are indicated by black and red lines, respectively. (E) Distances

664 between the mass centers of cells and colloidal gold are indicated by blue lines.

bioRxiv preprint doi: https://doi.org/10.1101/620922; this version posted April 28, 2019. The copyright holder for this preprint (which was not certified by peer review) is the author/funder, who has granted bioRxiv a license to display the preprint in perpetuity. It is made available under aCC-BY-NC-ND 4.0 International license.

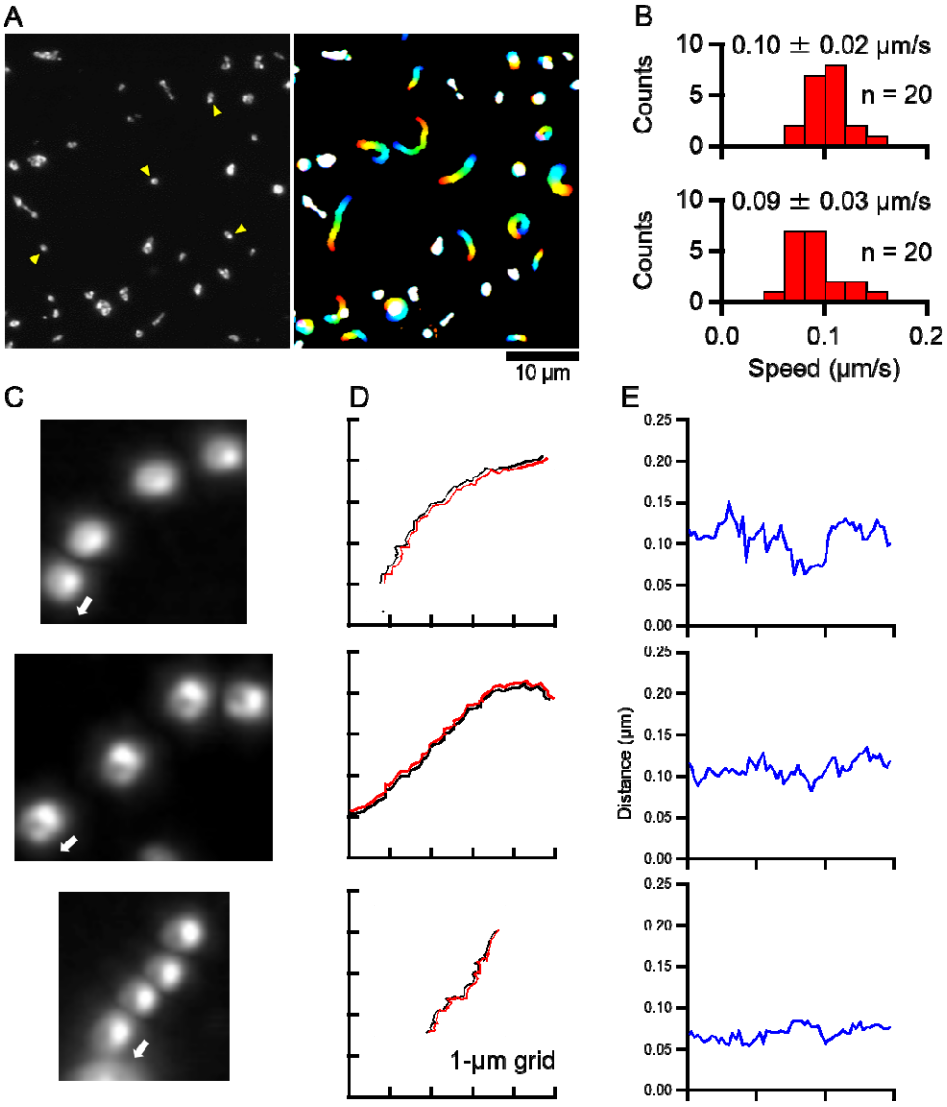

Fig. S2 Cells rotating around the end of the membrane protrusion under 0.5 mM SL. (A) Sequential phase-contrast micrographs of a cell at 1 s intervals. (B) The mass center of the cell was traced at 5 ms intervals for 30 s. (C) Time courses against the *X*-axis (upper) and *Y*-axis (lower) of panel B.

bioRxiv preprint doi: https://doi.org/10.1101/620922; this version posted April 28, 2019. The copyright holder for this preprint (which was not certified by peer review) is the author/funder, who has granted bioRxiv a license to display the preprint in perpetuity. It is made available under aCC-BY-NC-ND 4.0 International license.

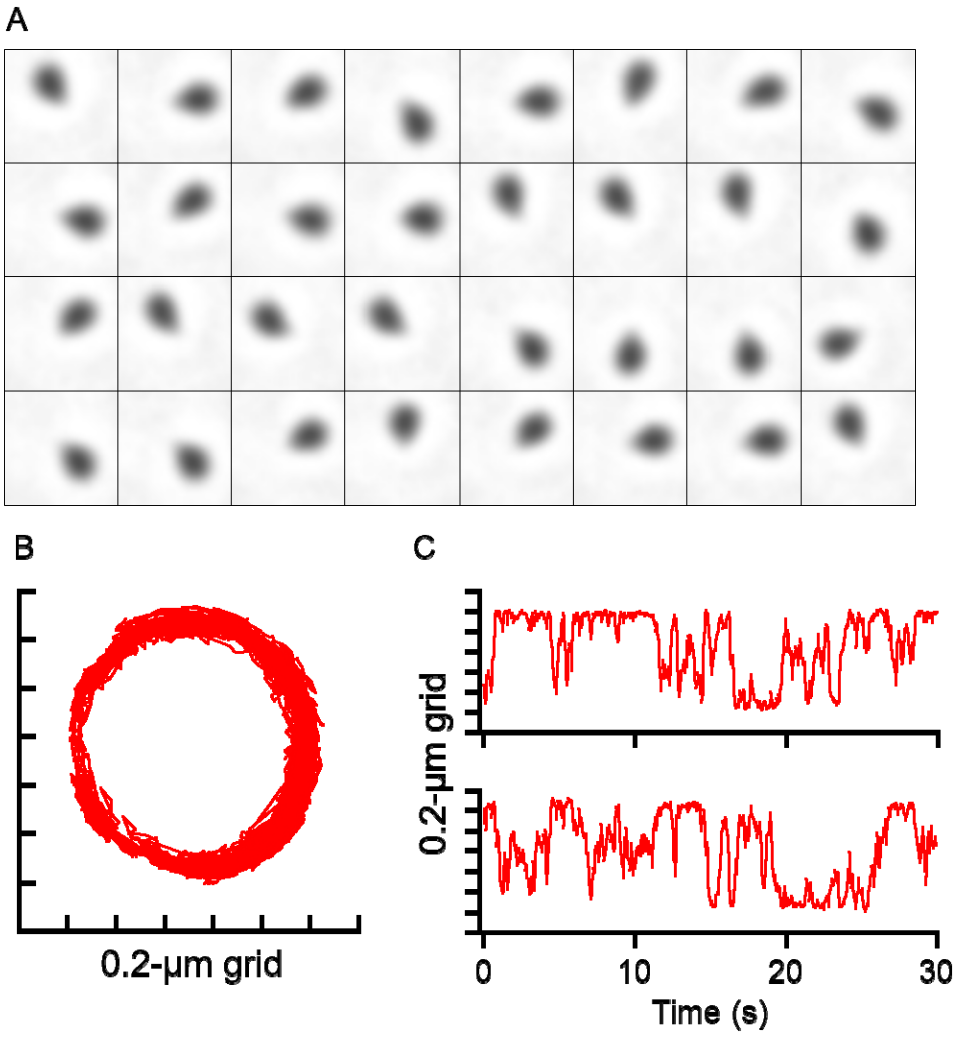

670

671

bioRxiv preprint doi: https://doi.org/10.1101/620922; this version posted April 28, 2019. The copyright holder for this preprint (which was not certified by peer review) is the author/funder, who has granted bioRxiv a license to display the preprint in perpetuity. It is made available under aCC-BY-NC-ND 4.0 International license.

672 Fig. S3

673 Hill plot analysis of data in Fig. 3C.

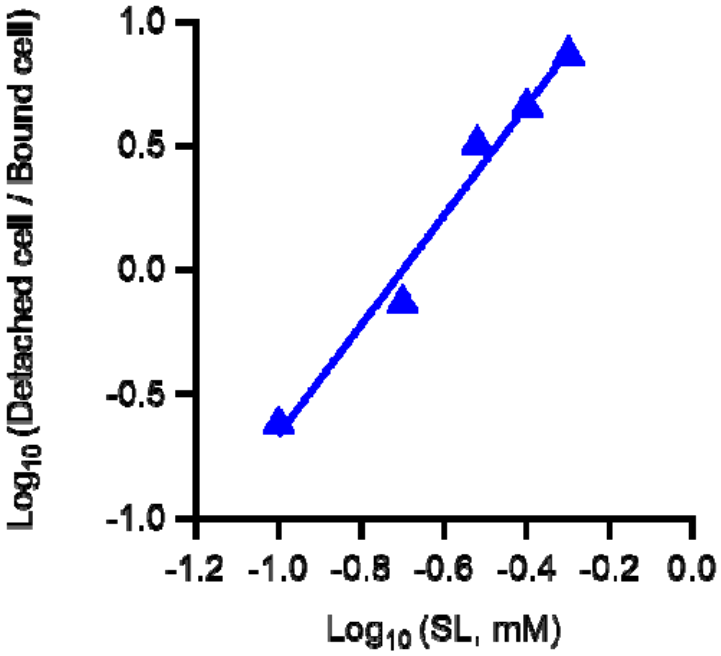

674

675

bioRxiv preprint doi: https://doi.org/10.1101/620922; this version posted April 28, 2019. The copyright holder for this preprint (which was not certified by peer review) is the author/funder, who has granted bioRxiv a license to display the preprint in perpetuity. It is made available under aCC-BY-NC-ND 4.0 International license.

676 Fig. S4 Gliding motility under bufferA.

677 (A) Field image of phase-contrast micrograph (left) and cell trajectories for 30 s,

678 changing color with time from red to blue (right). (B) Distribution of gliding speeds

679 averaged for 60 s under bufferA was fitted with a Gaussian curve. (C) Distribution of

680 gliding directions under bufferA was fitted with a Gaussian curve.

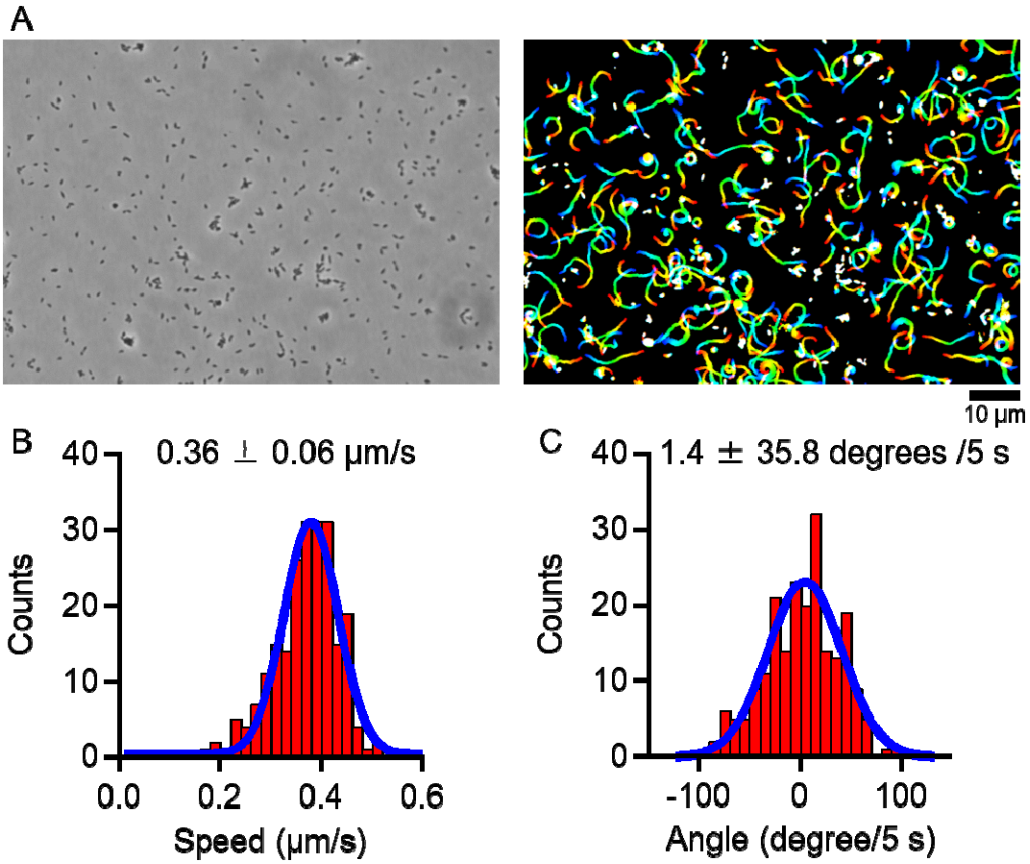

681

682

bioRxiv preprint doi: https://doi.org/10.1101/620922; this version posted April 28, 2019. The copyright holder for this preprint (which was not certified by peer review) is the author/funder, who has granted bioRxiv a license to display the preprint in perpetuity. It is made available under aCC-BY-NC-ND 4.0 International license.

683 Fig. S5 Transition of cell-image density in gliding ghost experiments.

684 (A) Distributions of cell-image densities at 30, 60, and 120 s after the addition of Triton

685 solution was fitted by the sum of two or three Gaussian curves. The individual Gaussian

686 curves and the sum of the Gaussian curves are indicated by black broken and magenta

687 solid lines, respectively. The cell-image density before Triton treatment is normalized as

688 100%. The positions of peak tops are indicated by black triangles. (B) Trajectories at 5 s

689 intervals of all cells (left) and the cell to be the gliding ghost (right). The color changes

690 with time from red to blue. The 0.007% Triton X-100 containing 1 mM ATP + 0.01 mM

691 ADP solution was added at 0 s. (C) Phase-contrast micrographs of intact (upper),

692 pre-permeabilized (middle) and post-permeabilized cells (lower). The time points after

693 the addition of Triton solutions are shown in each panel. (D) Transitions of gliding

694 speeds and cell-image densities. The average gliding speeds and cell-image densities for

695 10 s at 1 s intervals are plotted as black circles and gray triangles, respectively. The

696 average cell-image densities of the first 10 s are normalized as 100%. ‘Tri’ and ‘Per’

697 indicate that the time points when 0.007% Triton X-100 containing 1 mM ATP + 0.01

698 mM ADP solution was added, and the density shift occurred, respectively. Two

699 examples are shown for each category.

bioRxiv preprint doi: https://doi.org/10.1101/620922; this version posted April 28, 2019. The copyright holder for this preprint (which was not certified by peer review) is the author/funder, who has granted bioRxiv a license to display the preprint in perpetuity. It is made available under aCC-BY-NC-ND 4.0 International license.

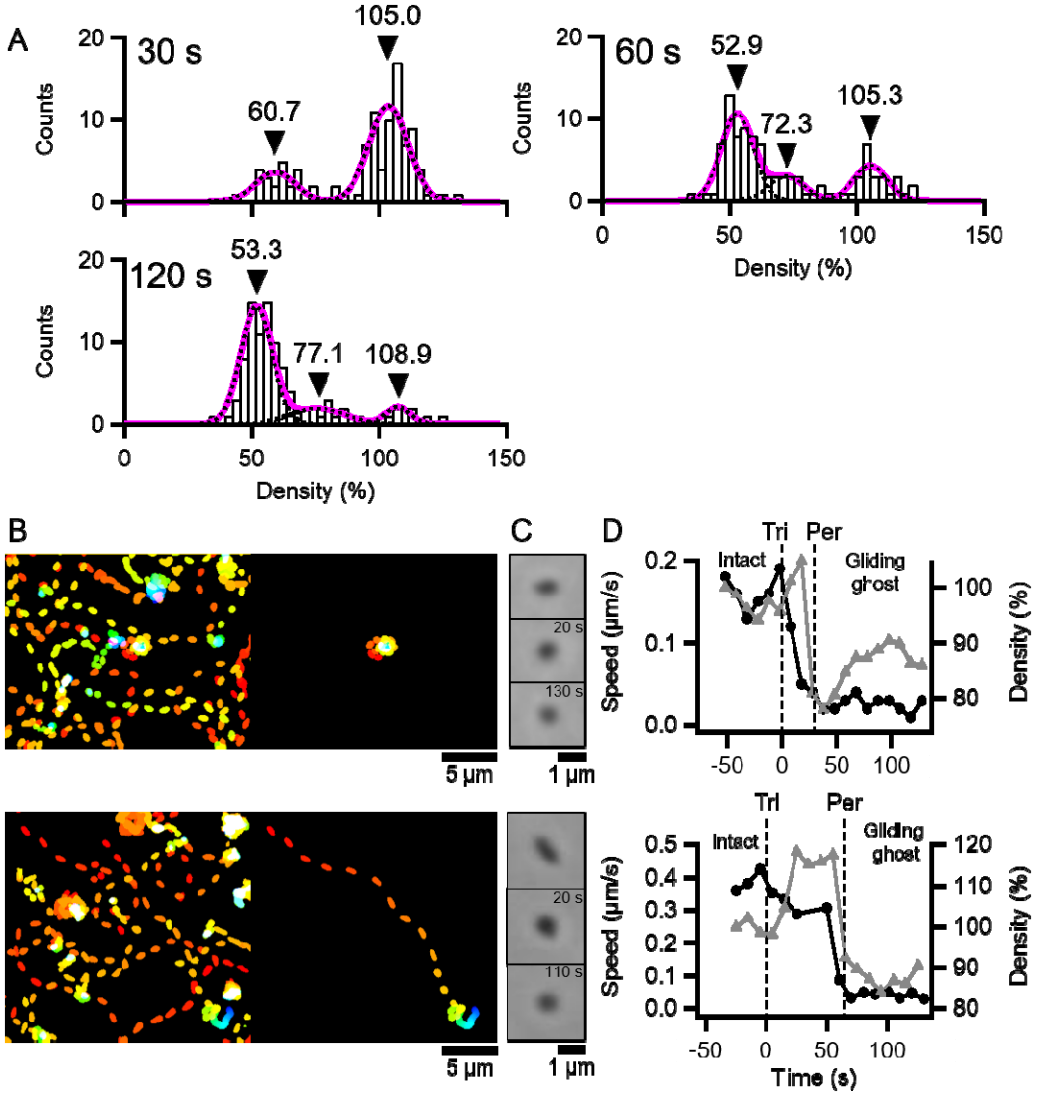

700

701

bioRxiv preprint doi: https://doi.org/10.1101/620922; this version posted April 28, 2019. The copyright holder for this preprint (which was not certified by peer review) is the author/funder, who has granted bioRxiv a license to display the preprint in perpetuity. It is made available under aCC-BY-NC-ND 4.0 International license.

Movie S1

Gliding *M. gallisepticum* under normal conditions. The movie is 5× speed.

Movie S2

Gliding *M. gallisepticum* attached with colloidal gold. The movie is 5× speed.

Movie S3

Gliding ghost of *M. mobile* under ATP. The movie is 2× speed.

Movie S4

Gliding ghost of *M. mobile* under ADP. The movie is 2× speed.

Movie S5

Gliding ghost of *M. gallisepticum* under ATP. The movie is 30× speed.